Supplement for "Influence of Tropospheric Temperature on the Formation and Aging of Secondary Organic Aerosol from Biogenic Vapor Mixtures"

Linyu Gao[1,2], Stella E. I. Manavi[3], Claudia Mohr[4,5], Junwei Song[1,2], Cheng Wu[6], Thomas Leisner[1,7], Spyros N. Pandis[3], and Harald Saathoff[1*]

[1] Institute of Meteorology and Climate Research, Karlsruhe Institute of Technology, Karlsruhe, 76344, Germany
[2] Now at: Université Claude Bernard Lyon 1, CNRS, IRCELYON, Villeurbanne, 69626, France
[3] Department of Chemical Engineering, University of Patras, Patras, 26504, Greece
[4] Department of Environmental Systems Science, ETH, Zurich, 8092, Switzerland
[5] PSI Center for Energy and Environmental Sciences, Paul Scherrer Institute, Villigen, 5232, Switzerland
[6] Department of Chemistry and Molecular Biology, University of Gothenburg, 41296, Gothenburg, Sweden
[7] Institute of Environmental Physics, Heidelberg University, Heidelberg, 69120, Germany

Correspondence to: Linyu Gao (linyugaoo@163.com) & Harald Saathoff (harald.saathoff@kit.edu)

Number of pages: 24
Number of sections:3
Number of figures: 14
Number of tables: 3

Section S1. Instruments, particle collection approach, and discussion of potential sampling artifacts in this work

S1.1 Instruments

SOA concentration was online detected by a high-resolution time-of-flight Aerosol Mass Spectrometer (HR-AMS, Aerodyne Inc.). The HR-AMS employs electron impact (EI) ionization, a hard ionization method that induces extensive fragmentation of organic molecules, being able to provide quantitative information on the bulk mass of organic aerosol but lacks molecular-level information. In addition, the particle-phase chemical composition of SOA was detected by a chemical ionization mass spectrometer (CIMS) coupled with a filter inlet for gas and aerosols (FIGAERO) using iodide (I^-) as reagent ions with 1 Hz time resolution(Lopez-Hilfiker et al., 2014; Lee et al., 2014). FIGAERO-iodide-CIMS uses a soft ionization technique that is highly sensitive to polar and oxygenated organic compounds. Consequently, the organic aerosol components detected by CIMS represent a subset of the total organic aerosol, specifically those that are oxygenated organic compounds (Lee et al., 2014). The chemical composition measured by the HR-AMS and FIGAERO-iodide-CIMS is expected to be consistent, as the nature of SOA is oxygenated. However, the sensitivity of FIGAERO-iodide-CIMS towards different organic compounds varies significantly, inhibiting a quantification of individual molecules or the sum of the compounds detected by FIGAERO-iodide-CIMS without extensive calibration.

Data analysis was done using Tofware 3.2.2 (Aerodyne). Note that the reagent ion I^- (m/z = 126.904) was subtracted from the molecular mass weights presented in this work. The mass resolution of FIGAERO-CIMS was 4000. Formulas were assigned with a mass accuracy of better than 20 ppm based on the mass resolution. We also note that the sensitivity of FIGAERO-iodide-CIMS is highly dependent on the functionalities of the organic compounds and can vary by orders of magnitudes(Lopez-Hilfiker et al., 2016a; Lee et al., 2014; Riva et al., 2019). Therefore, the results shown in this work are based on signal intensities but not mass concentrations.

S1.2 Particle collection approach

The particle data presented in this work stems from offline analysis. Particles were collected on Polytetrafluorethylene (PTFE, 1 μm, SKC Inc.) filters with a sampling flow of 6.4 L/min for 5 minutes, when particle concentrations stabilized during the experiments. The number of samples obtained at each temperature was as follows: one at 213 K, three at 243 K, and two each at 273 K, 298 K, and 313 K. In addition, one filter was sampled after warming was completed. The filter samples were analyzed using a FIGAERO-iodide-CIMS. Thermal desorption was performed under a flow of ultra-high-purity nitrogen as the carrier gas. The temperature was first ramped from 296 K to 473 K over 15 min and then held at 473 K for an additional 20 min, resulting in a total desorption time of 35 min(Lopez-Hilfiker et al., 2016a; Lee et al., 2014; Riva et al., 2019).

S1.3 Discussion of potential sampling artifacts in this work

The filter sampling setup and all instruments were installed in the laboratory outside the chamber at room temperature (295±2 K). To minimize the effect of temperature differences between the chamber temperatures (213 K, 243 K, 273 K, 298 K, 313 K) and room temperature on the gas-phase chemical composition, the sampling line to the CIMS was partially insulated and the residence time in the Teflon sampling line was only 2 s. The residence time in the stainless-steel line for filter sampling was about 1 s. The sampling time of Telflon filters at all experiments were typically 5 minutes plus a few minutes of handling time before the sample

was stored in the freezer (-20 °C). We ever characterized the potential losses of semi-volatile VOCs during the particle collection, storage, and thermal analyses, and compared thermograms from filters that were collected (5 min) and analyzed immediately with those that were collected and stored frozen for several days before analysis. These tests demonstrated the effect of evaporation on most oxygenated organic compounds can be negligible(Huang et al., 2018; Gao et al., 2022a; Gao et al., 2023).

Another potential artefact is thermal decomposition during the thermal desorption analyses. Thermal degradation is a known phenomenon in FIGAERO measurements, primarily associated with higher desorption temperatures (e.g., >100 °C)(Lopez-Hilfiker et al., 2014; Stark et al., 2017) rather than the duration of the process itself. We checked the thermal desorption profiles for each compound, and found not much compounds showing high T_{max} values (e.g., > 100 °C), shown as Figure S1. This indicates the effect of thermal decomposition is limited to the chemical composition of particles presented in this work.

The residence time in the stainless-steel sampling line to the HR-AMS was 4 s, allowing the sample air to warm up before entering the instrument. Hence, we cannot fully exclude some particle evaporation and there could be an underestimation of the more volatile fraction of the particles in the HR-AMS measurements.

Section S2. Description of PMCAMx simulations of the biogenic SOA concentrations over Europe.

The chemical transport model PMCAMx simulates atmospheric processes such as horizontal and vertical advection, horizontal and vertical dispersion, wet and dry deposition, gas and aqueous-phase chemistry, aerosol dynamics and thermodynamics(Murphy and Pandis, 2009; Tsimpidi et al., 2010; Fountoukis et al., 2011). For the gas-phase chemistry, the model utilizes a modified version of the SAPRC gas-phase mechanism(Carter, 2000), which includes overall 237 reactions of 91 gases and 18 radicals. Biogenic volatile organic compounds (VOCs) are simulated with three gas phase species, isoprene, one lumped terpenes species and one lumped sesquiterpenes species. For the simulation of aerosol processes in this application, bulk equilibrium is assumed. Moreover, the model treats both the primary (POA) and secondary organic aerosol (SOA) as semi-volatile and chemically reactive. Specifically, the SOA volatility basis-set methodology(Lane et al., 2008) is employed to simulate the formation of SOA from anthropogenic and biogenic precursors. The oxidation reactions of the three biogenic precursors lead to the formation of a set of four semi-volatile species with a saturation concentration (C* in $\mu g\ m^{-3}$) of 1, 10, 100, 1000. For both anthropogenic and biogenic SOA, the SOA module utilizes NO_x-dependent SOA yields that are based on previous smog-chamber experimental results(Ng et al., 2006). The NO_x-dependent mass-based stoichiometric yields utilized in the Base case and the New case are included in Tables S1 and S2.

The simulation period (5 June – 8 July 2012) corresponds to a field campaign measurement that took place in Po Valley, Northern Italy, as part of the Pan-European AeroSOls-climate interaction Study (PEGASOS). During the campaign, a number of HR-ToF-AMS (High-Resolution Time-of-Flight Aerosol Mass Spectrometer, Aerodyne Research) units were deployed at multiple ground sites across the Po Valley (Figure S4). The ground stationary measurements were performed at Bologna (BO, 44° 31’ 28” N, 11° 20’ 19” E), an urban background site in the southeastern part of the Po Valley; San Pietro Capofiume (SPC, 44° 39’ 15” N, 11° 37’ 29” E), a rural background site located in a sparsely populated flat countryside surrounded by kilometers of flat lands, 40 km northeast of Bologna; Monte Cimone (MTC, 44°12' N, 10°42' E, 2165 m a.s.l.) GAW station, located on the top of the highest peak of the northern Apennines; and Bosco Fontana (BF, 45°12’ N, 10°44’ E), a National Natural Reserve in Lombardy, in the middle of the valley.

Section S3. Temperature-dependent overall chemical composition and volatility of fresh SOA formed from the oxidation of mixtures of isoprene and α-pinene

The thermal desorption technique employed by FIGAERO-CIMS provides volatility information of individual SOA molecules based on their evolution changes as a function of the temperature during thermal desorption from particles. Different compounds have distinct responses to the desorption temperatures due to their different evaporation enthalpies and saturation vapor pressures(Lopez-Hilfiker et al., 2014; Thornton et al., 2020; Stark et al., 2017; Bannan et al., 2019). Such thermal profiles of individual compounds are regarded as thermograms. Thus, temperature at the peak of thermograms (hereafter 'T_{max}') is regarded as a qualitative indicator of volatility of SOA particles(Stark et al., 2017; Lopez-Hilfiker et al., 2016b). Figure S7 (a) shows the thermograms of SOA formed at 213 – 313 K, respectively. For each experiment, the reproducible thermograms of two particle samples collected successively indicate the low variability in the measurements. In this study, except for the experiments at 273 K and 243 K, the particles formed at higher temperatures tend to have higher T_{max}, suggesting decreasing volatilities. This is because higher temperatures lead to higher signal fractions of highly oxygenated molecules, from 13% at 273 K to 25% at 313 K. However, a lower T_{max} appears for the particles formed at 273 K, indicating that the oxygenated products formed at 273 K correspond to relatively higher volatile components. This picture is consistent with the volatility distribution using molecular saturation concentrations at 298 K ($\log C_{sat,298K}$, Figure S8) calculated from elemental formulas(Yang et al., 2023; Li et al., 2016; Lopez-Hilfiker et al., 2016b; Gao et al., 2023) ruling out the effect of SOA formation temperatures on shifting volatility bins. Illustrated in Figure S8, particles formed at 273 K are most volatile with the highest signal fraction (91 %) of intermediate-volatile and semi-volatile compounds among all particles. We note that 273 K is a critical temperature for biogenic SOA formation above/below where the temperature-dependence on chemical composition and volatility of SOA is different. This can be found also in SOA formation from β-caryophyllene oxidation(Gao et al., 2022b; Gao et al., 2023). While we currently lack definitive explanations for this phenomenon, the phase state is inferred to be a potential factor. Therefore, further studies are necessary to investigate the underlying mechanism. Figure S7 (b-f) illustrates that the volatility distribution of SOA compounds formed at lower temperatures (213 K, 243 K) is broader because of their wider component distribution including a higher fraction of dimers. For the wide temperature range studied here, a substantial shift of volatility bins after considering SOA formation temperatures proves that temperature has a larger impact on the volatility of particles via promoting phase partitioning, significantly beyond the effect of chemistry, in agreement with studies for other BVOC systems(Gao et al., 2023; Ye et al., 2019). Based on this method to determine SOA compound volatility, all compounds in the α-pinene isoprene derived SOA particles at 213 K should have a low volatility (LVOC, $-4.5 < \log_{10}C_{sat} < -0.5$) or less. With experiment temperatures increasing, the sum of the fractions of semi VOC (SVOC, $-0.5 < \log_{10}C_{sat} < 2.5$) and intermediate VOC (IVOC, $2.5 < \log_{10}C_{sat} < 6.5$) increase from 1.1 % (243 K) to 90.8 % (313 K).

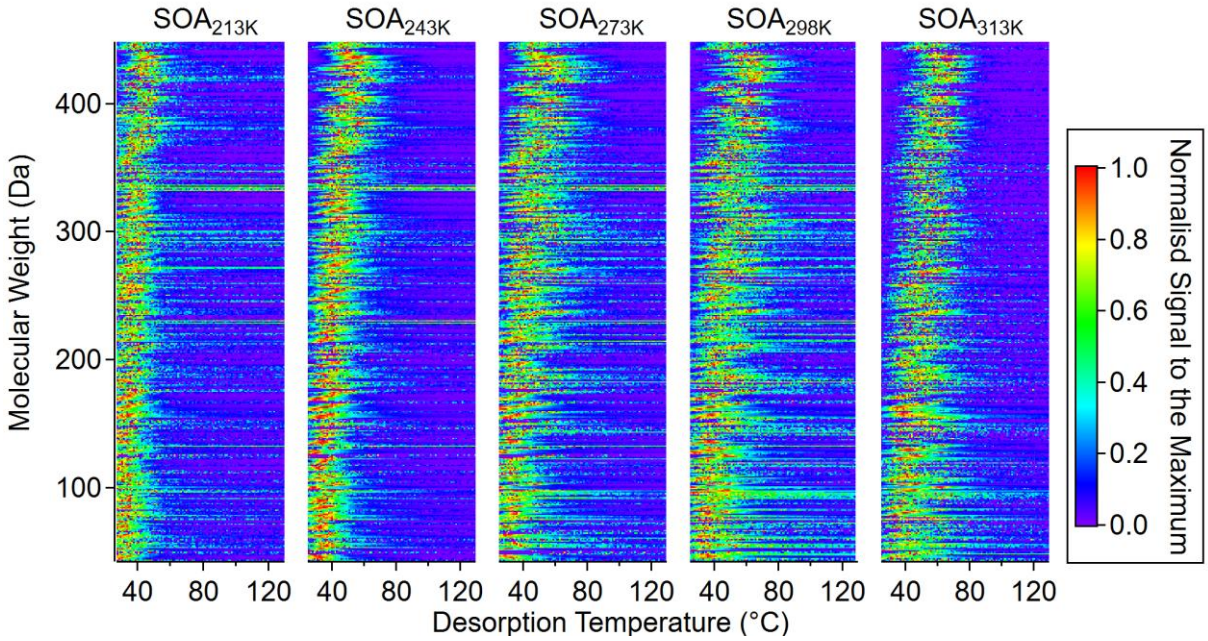

Figure S1. Two-dimension thermal desorption profiles of all detected molecules in the particles (SOA_{213K}, SOA_{243K}, SOA_{273K}, SOA_{298K}, SOA_{313K}).

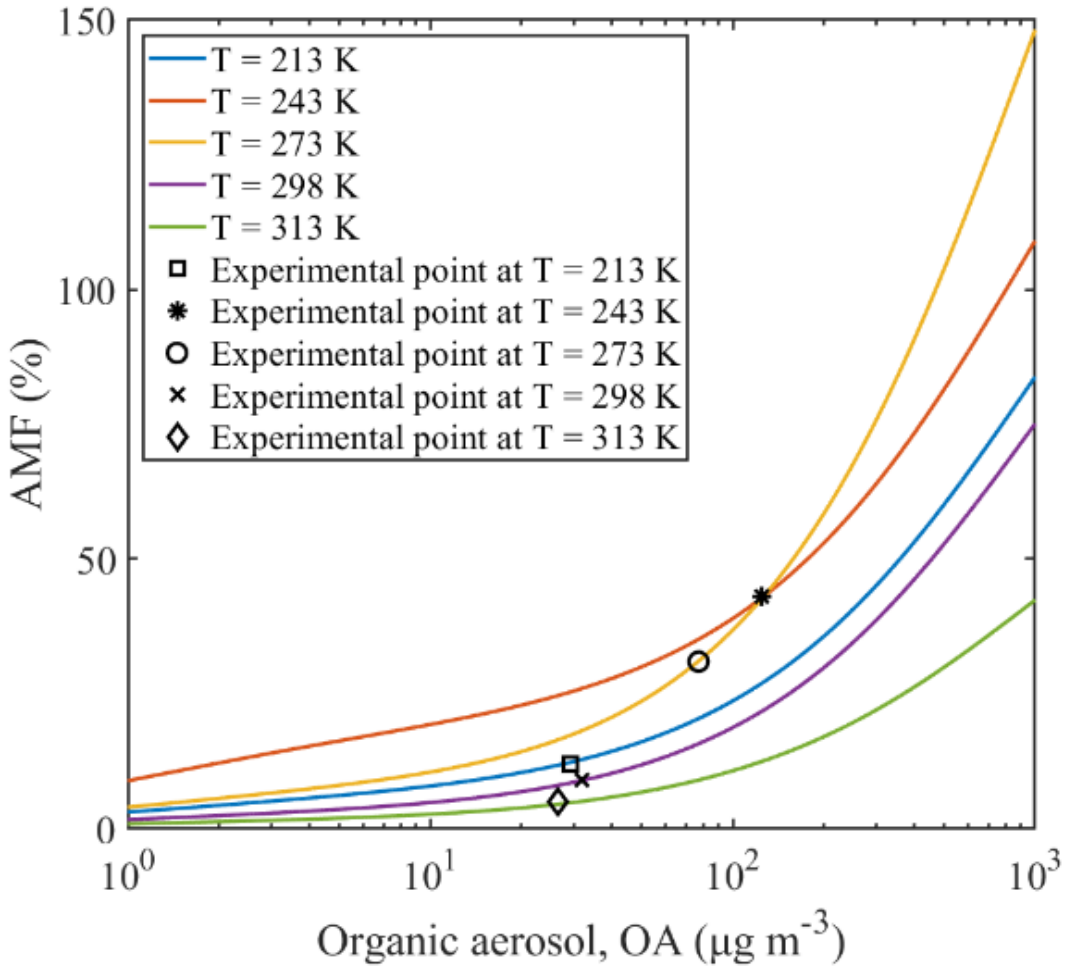

Figure S2. Aerosol mass fraction (yield) corresponding as a function of organic aerosol concentration used as inputs in the PMCAMx simulation. Also shown are the corresponding measurements.

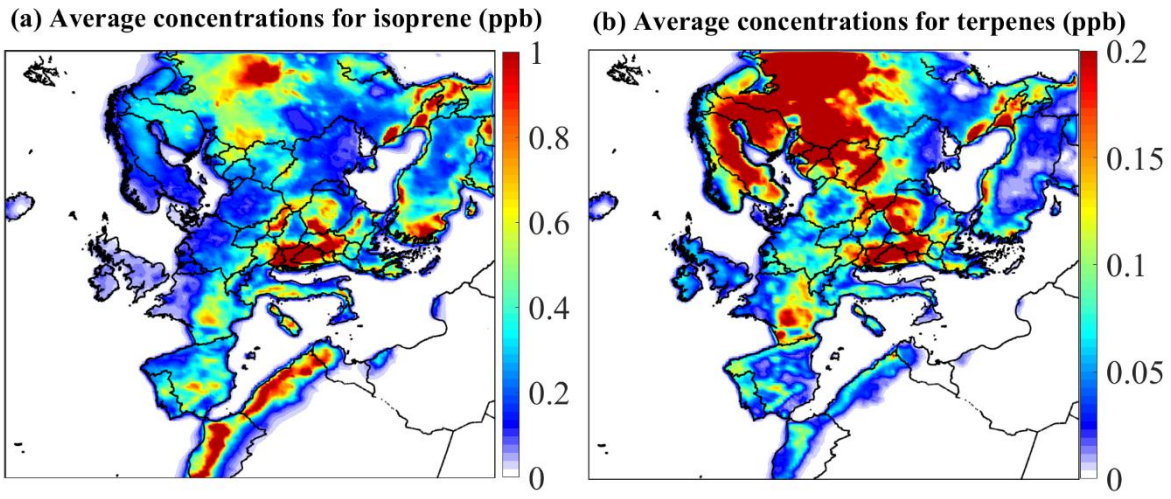

Figure S3. Monthly average concentrations of isoprene (left, in ppb) and terpene (right, in ppb) over Europe predicted by the "base case" simulation for the summer simulation period of PEGASOS 2012.

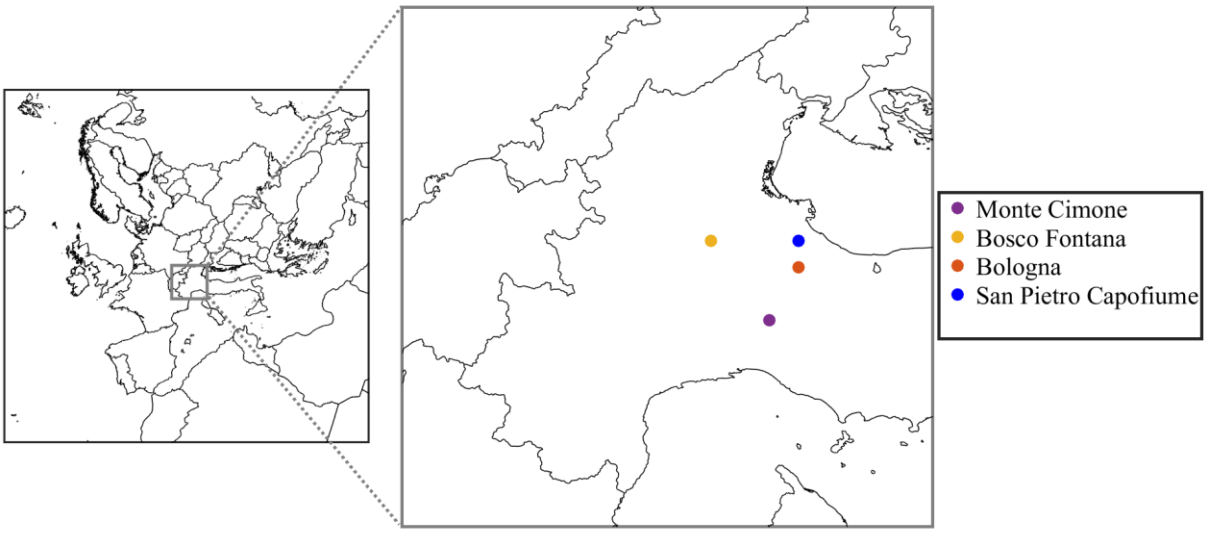

Figure S4. Modelling domain and the locations of the measuring sites in Italy.

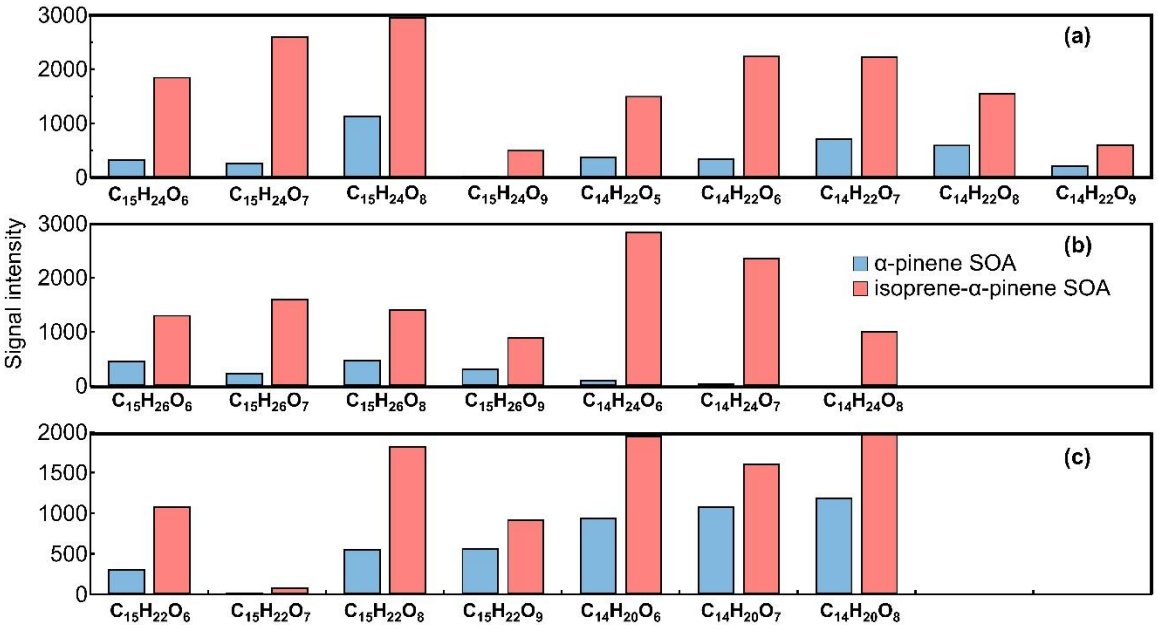

Figure S5. Comparison of $C_{14\text{-}15}$ dimers between Exp 0 (sole α-pinene) and Exp 3 (mixture of isoprene and α-pinene) at 273 K. Blue and red bars show the compound groups in the α-pinene SOA and isoprene-α-pinene SOA, respectively. Signals are normalised to the reagent ion (I^-) to 1e6 ions. a) potentially from $_{iso,O3}RO_2$ + $_{ap,OH}RO_2$ or $_{iso,OH}RO_2$ + $_{ap,O3}RO_2$; b) potentially from $_{iso,OH}RO_2$ + $_{ap,OH}RO_2$; c) potentially from $_{iso,O3}RO_2$ + $_{ap,O3}RO_2$.

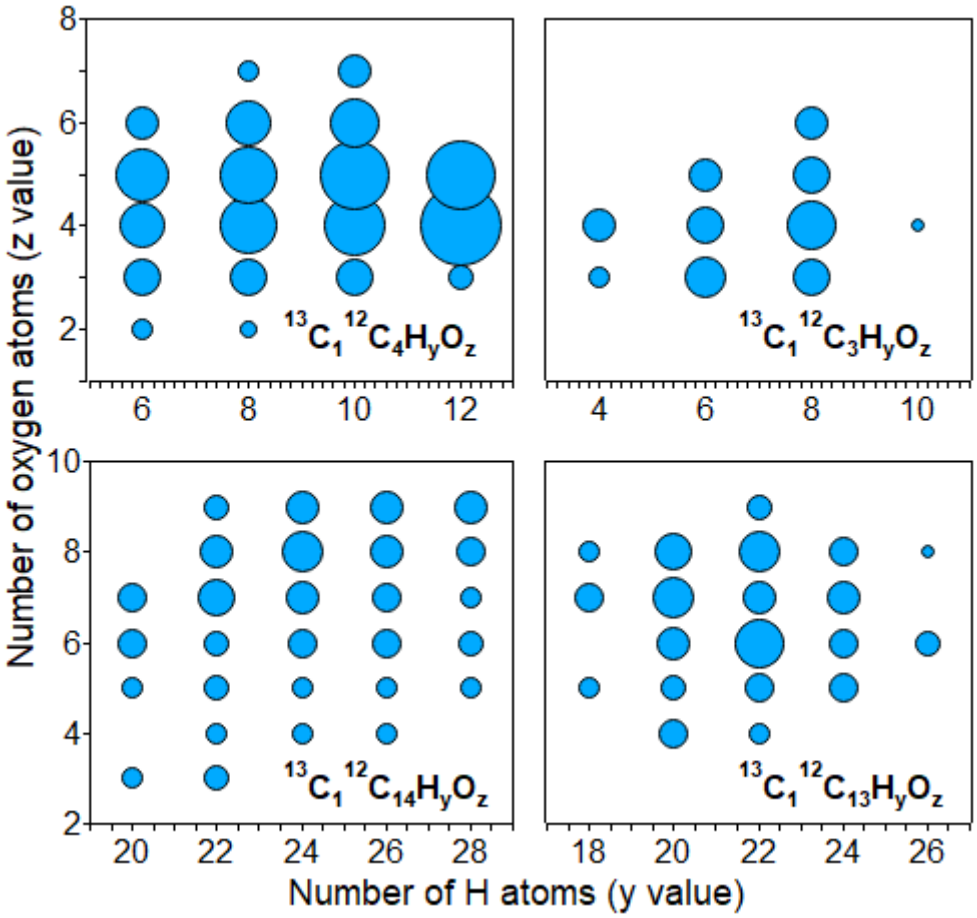

Figure S6. Oxidation compounds containing one ^{13}C atom defined from Exp 6 (α-pinene and ^{13}C labelled isoprene mixture). Symbol sizes are related to normalised signal abundance of each compound.

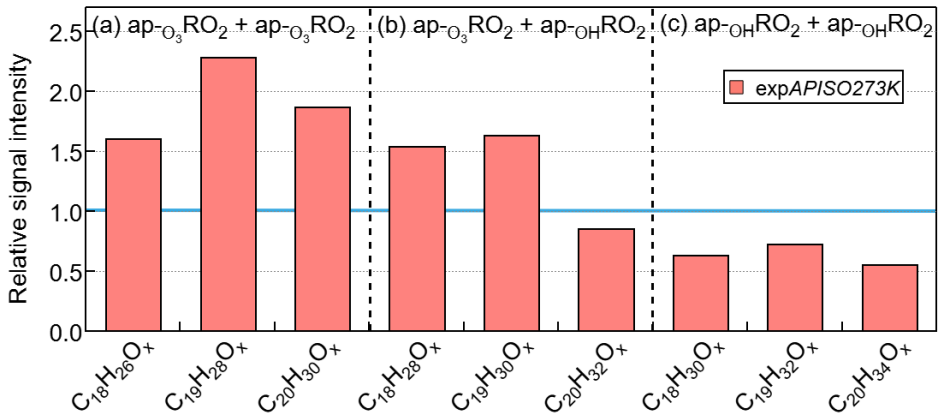

Figure S7. Relative signal intensity of α-pinene dimers ($C_{18\text{-}20}$) in newly formed α-pinene SOA at 273K in the presence of isoprene to the particles derived from sole α-pinene oxidation (blue line). Signals are normalised to the total signal amount of a) sum of $C_{18}H_{26}O_x$, $C_{19}H_{28}O_x$, $C_{20}H_{30}O_x$, and b) $C_{18}H_{28}O_x$, $C_{19}H_{30}O_x$, $C_{20}H_{32}O_x$, and c) $C_{18}H_{30}O_x$, $C_{19}H_{32}O_x$, $C_{20}H_{34}O_x$.

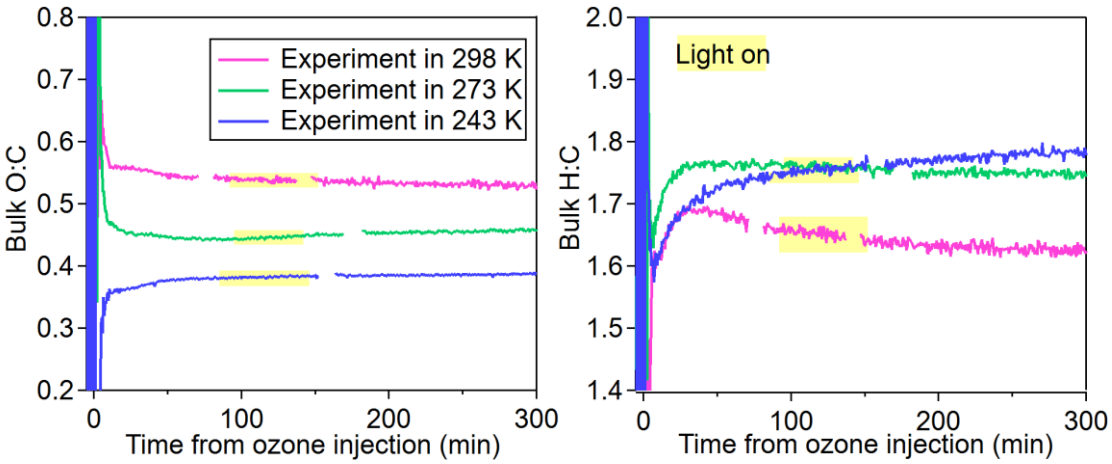

Figure S8. Timeseries of O:C and H:C values of bulk particles measured by HR-AMS during illumination period.

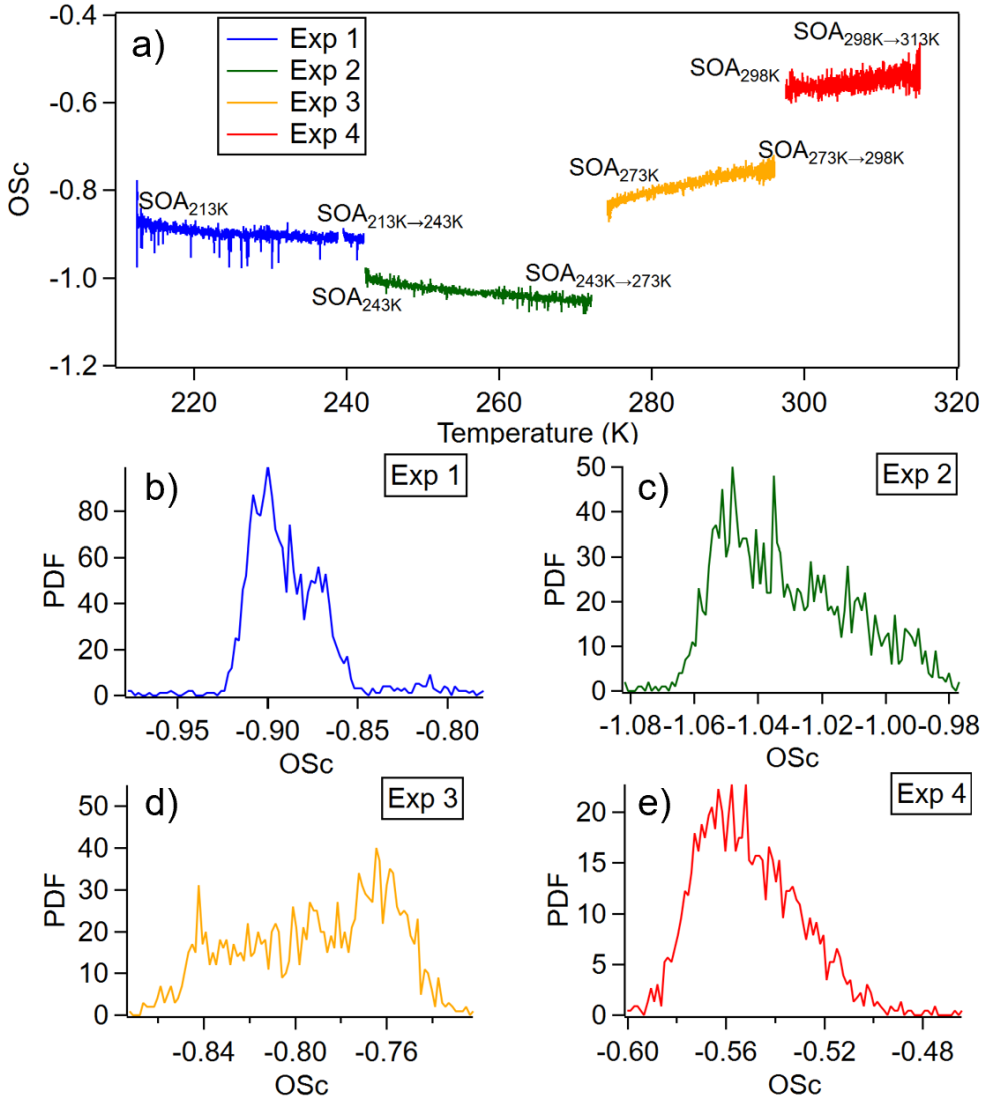

Figure S9. (a) Evolution of carbon oxidation state (OS_C) across temperatures during warming periods of different experiments (Exp 1-4). (b-e) probability density function plots of OS_C during each experiment (based on HR-ToF-AMS data).

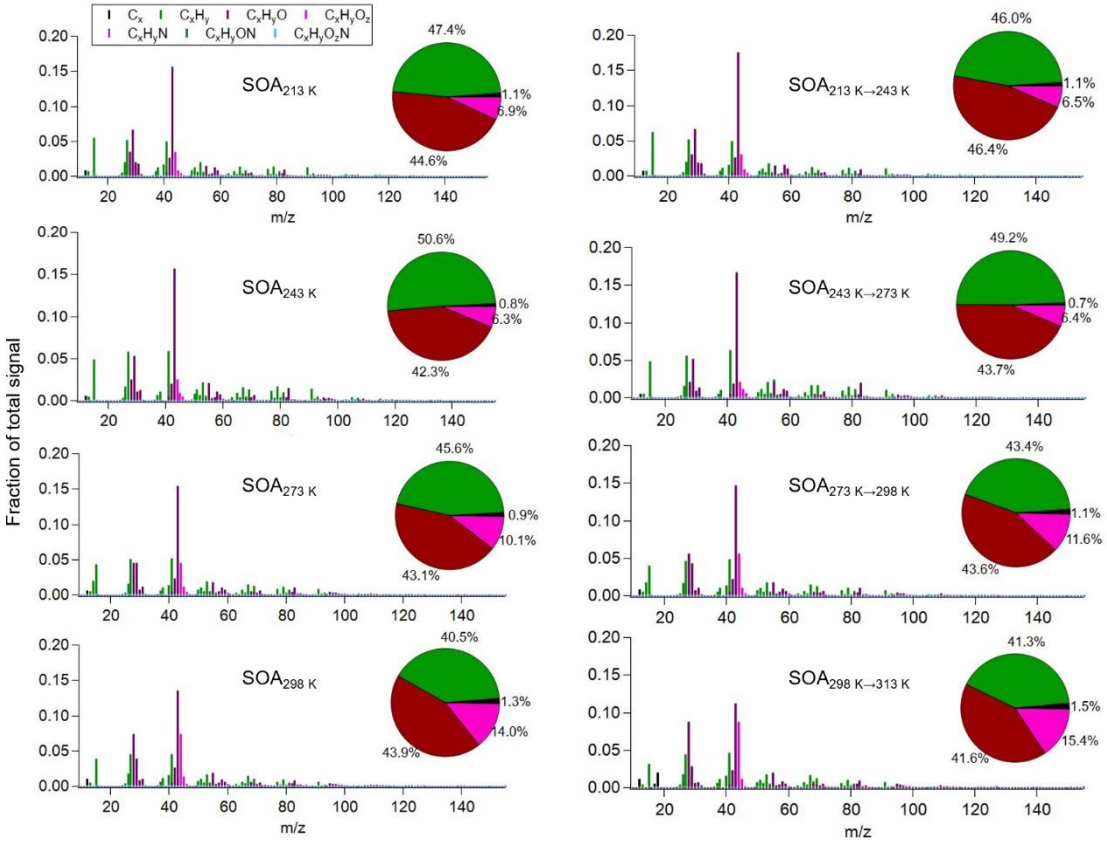

Figure S10 . Chemical composition of the fresh SOA (left) and the SOA after warming (right) measured by HR-ToF-AMS. The pie charts show the bulk chemical information, including organic-related fragments (grouped as C_x, $C_xH_y^+$, $C_xH_yO^+$, $C_xH_yO_z^+$, $C_xH_yN^+$, $C_xH_yON^+$ and $C_xH_yO_zN^+$, where x, y, z ≥ 1). Large portions of hydrocarbon-like (indicated by $C_xH_y^+$), less oxygenated fragments (indicated by $C_xH_yO^+$), and higher oxygenated fragments (indicated by $C_xH_yO_z^+$) are observed.

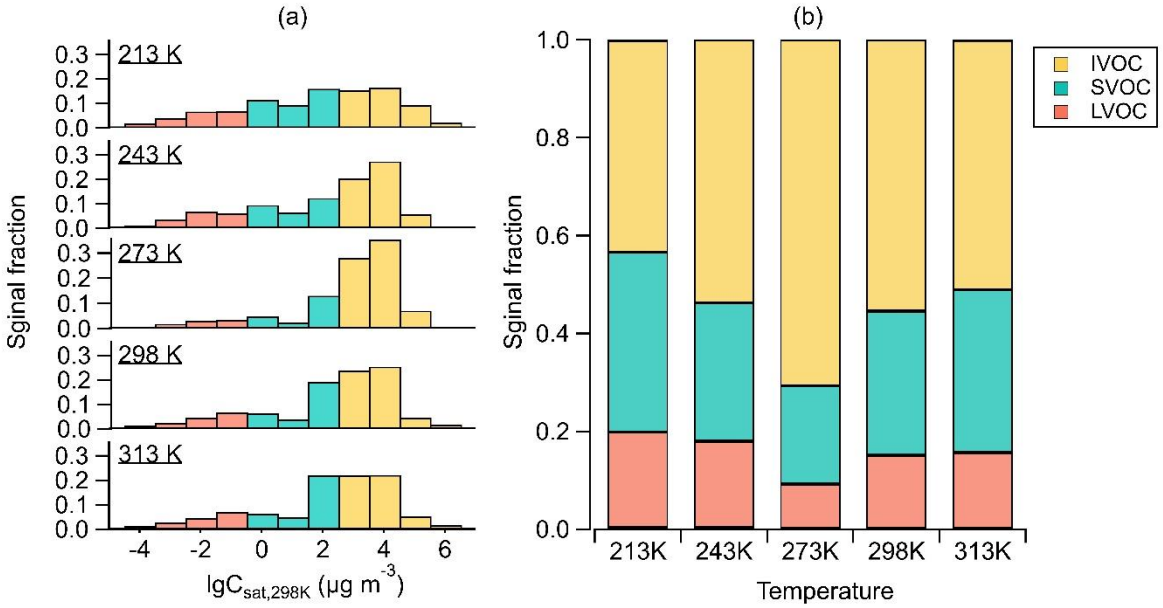

Figure S11. a) Volatility distribution of fresh particles formed at all temperatures corresponding to 298 K saturation concentrations, and b) their fraction the volatility bins: ULVOC, ELVOC, LVOC, SVOC, IVOC, and VOC identified based on the saturation concentrations as described in the Method. Please note that $lgC_{sat,298K}$ refer to saturation concentrations at 298 K, which is different from the $\log_{10}C_{sat,T}$ which are related to their formation temperatures.

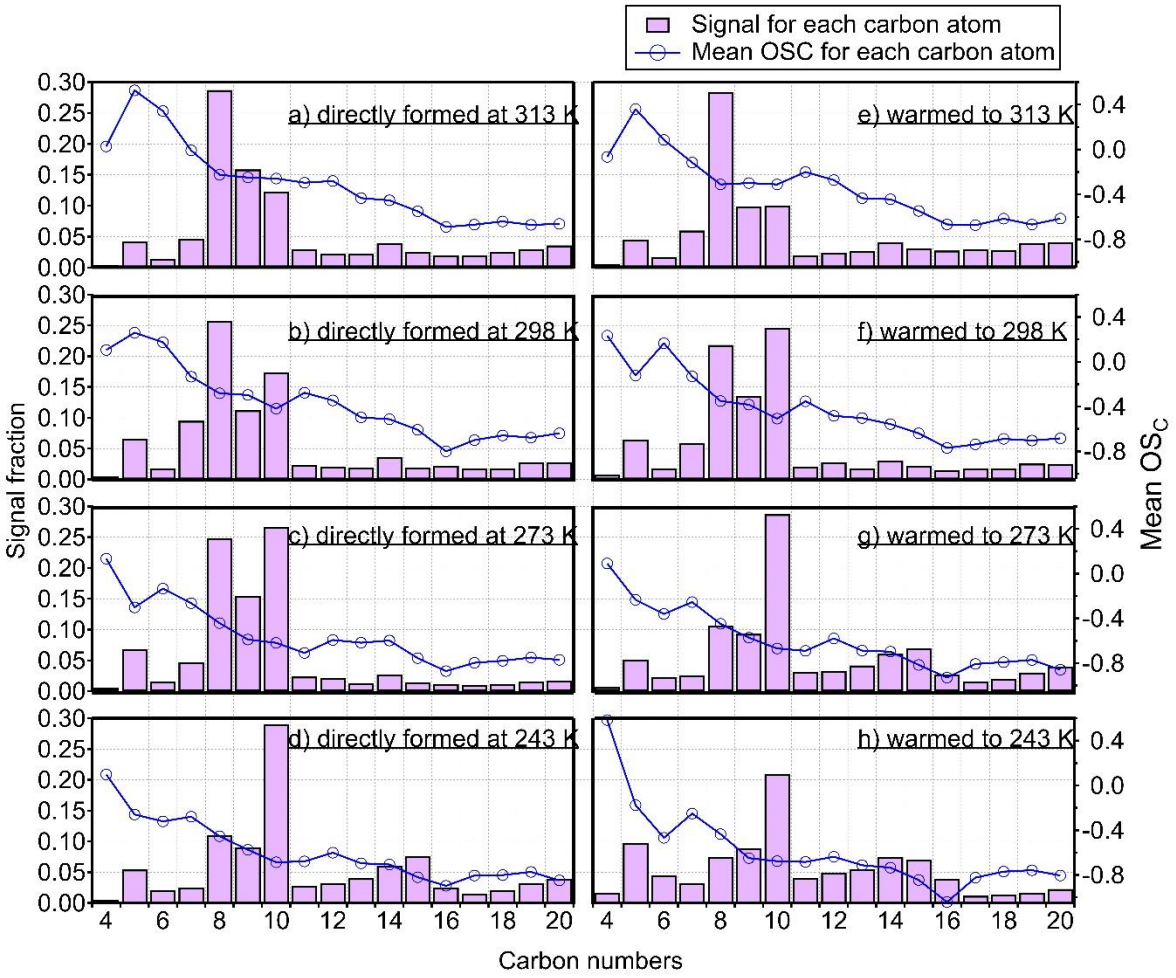

Figure S12. Signal fraction of particle-phase products corresponding to carbon numbers for particles formed directly at 313 K (a), 298 K (b), 273 K (c), 243 K (d), and particles warmed to 313 K (e), 298 K (f), 273 K (g), 243 K (h), as well as the averaged OS_C values of each carbon group (circles and solid lines).

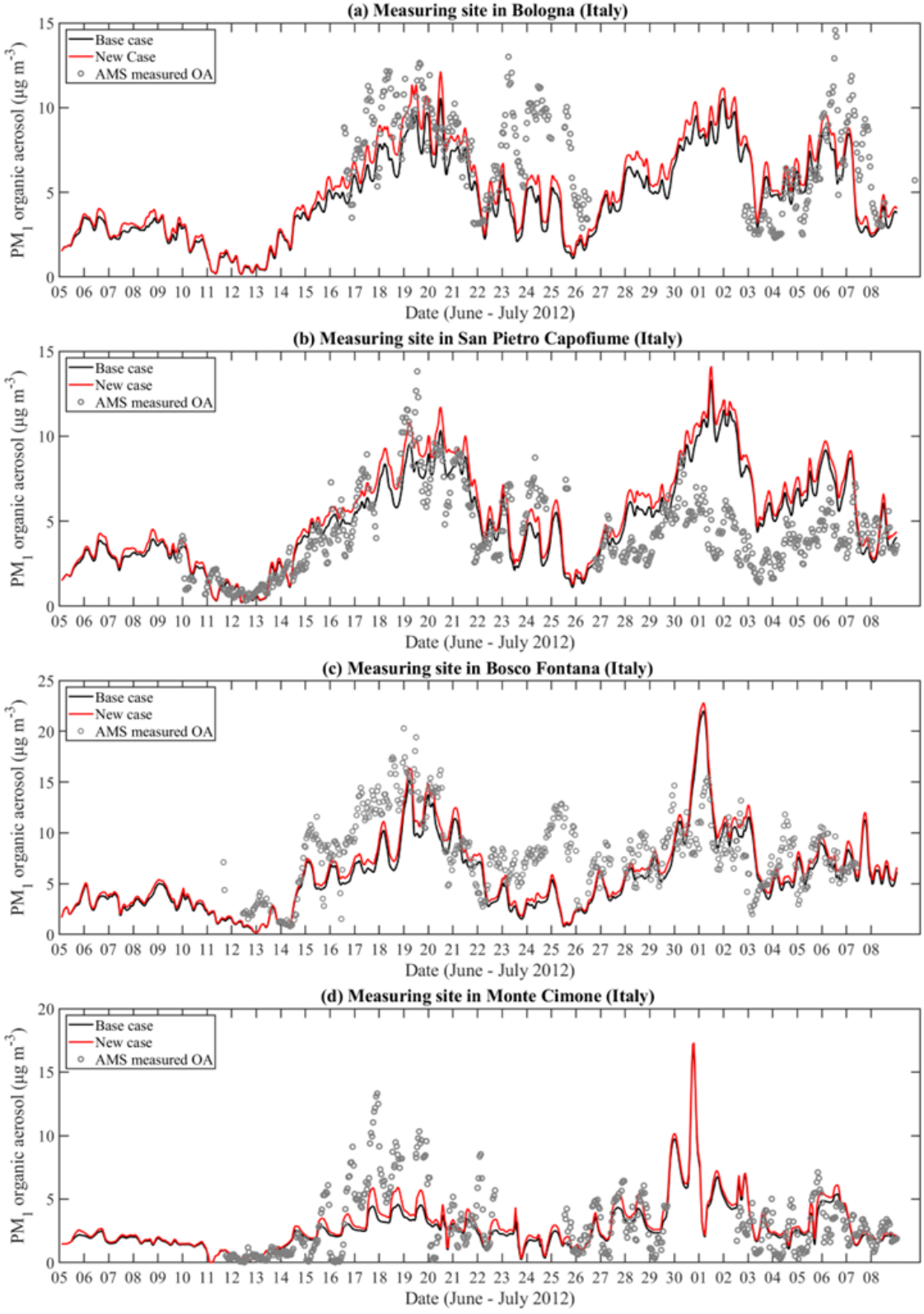

Figure S13. Ground level hourly concentrations of PM_1 organic aerosol as predicted by the Base case and the New case compared against AMS measurements taken at the 4 measuring sites. From top to bottom: Bologna, San Pietro Capofiume, Bosco Fontana, and Monte Cimone.

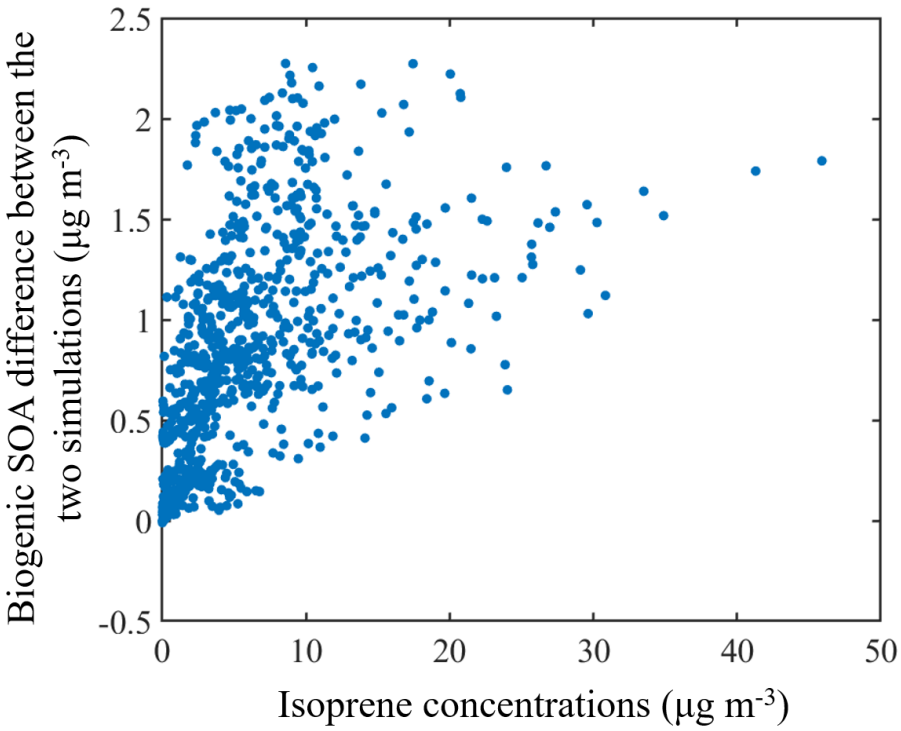

Figure S14. The difference of biogenic SOA concentrations between the two simulations for the simulation cell over Croatia are plotted against the hourly average concentrations of isoprene for the same cell.

Table S1. Mass-based stoichiometric yields utilized in the "Base case" scenario to simulate biogenic SOA formation from isoprene and terpenes.

Species Name	Mass based stoichiometric yields (a_i) (%) at 298 K with			
	C* = 1 μg m^{-3}	C* = 10 μg m^{-3}	C* = 100 μg m^{-3}	C* = 1000 μg m^{-3}
Isoprene	0.9	3	1.5	0
Terpenes	10.73	9.18	35.87	60.75

Table S2. Mass-based stoichiometric yields utilized in the "New case" scenario to simulate biogenic SOA formation from isoprene and terpenes.

Temperature of the experiment	Mass based stoichiometric yields (a_i) (%) with			
	C* = 1 μg m^{-3}	C* = 10 μg m^{-3}	C* = 100 μg m^{-3}	C* = 1000 μg m^{-3}
213 K	5.4	1.7	8.5	137.9
243 K	16.7	3.5	9.4	160.8
273 K	7.1	1.2	9.9	261.8
298 K	2.9	0.6	7	130.5
313 K	1.5	0.3	4.7	72.6

Table S3. Summary of O:C, H:C, OSC values of all SOA particles measured by HR-AMS and FIGAERO-iodide-CIMS.

Particles	HR-AMS measurement			FIGAERO-iodide-CIMS measurement		
	O:C ratios	H:C ratios	OS_C	O:C ratios	H:C ratios	OS_C
SOA_{213K}	0.45	1.79	-0.89	0.55	1.66	-0.56
$SOA_{213K→243K}$	0.47	1.84	-0.90	0.57	1.68	-0.54
SOA_{243K}	0.36	1.69	-0.97	0.50	1.63	-0.63
$SOA_{243K→273K}$	0.40	1.82	-1.02	0.50	1.62	-0.62
SOA_{273K}	0.44	1.76	-0.87	0.54	1.60	-0.52
$SOA_{273K→298K}$	0.48	1.73	-0.75	0.57	1.55	-0.41
SOA_{298K}	0.53	1.63	-0.57	0.60	1.51	-0.31
$SOA_{298K→313K}$	0.52	1.57	-0.53	0.59	1.49	-0.31
SOA_{313K}	0.54	1.57	-0.49	0.60	1.47	-0.27

References

Bannan, T. J., Le Breton, M., Priestley, M., Worrall, S. D., Bacak, A., Marsden, N. A., Mehra, A., Hammes, J., Hallquist, M., Alfarra, M. R., Krieger, U. K., Reid, J. P., Jayne, J., Robinson, W., McFiggans, G., Coe, H., Percival, C. J., and Topping, D.: A method for extracting calibrated volatility information from the FIGAERO-HR-ToF-CIMS and its experimental application, Atmos. Meas. Tech., 12, 1429-1439, 10.5194/amt-12-1429-2019, 2019.

SAPRC-99 Mechanism Files and Associated Programs and Examples: https://intra.cert.ucr.edu/~carter/SAPRC99/index.htm, last access: 12 Nov.

Fountoukis, C., Racherla, P. N., Denier van der Gon, H. A. C., Polymeneas, P., Charalampidis, P. E., Pilinis, C., Wiedensohler, A., Dall'Osto, M., O'Dowd, C., and Pandis, S. N.: Evaluation of a three-dimensional chemical transport model (PMCAMx) in the European domain during the EUCAARI May 2008 campaign, Atmos. Chem. Phys., 11, 10331-10347, 10.5194/acp-11-10331-2011, 2011.

Gao, L., Song, J., Mohr, C., Huang, W., Vallon, M., Jiang, F., Leisner, T., and Saathoff, H.: Kinetics, SOA yields, and chemical composition of secondary organic aerosol from β-caryophyllene ozonolysis with and without nitrogen oxides between 213 and 313 K, Atmos. Chem. Phys., 22, 6001-6020, 10.5194/acp-22-6001-2022, 2022a.

Gao, L., Song, J., Mohr, C., Huang, W., Vallon, M., Jiang, F., Leisner, T., and Saathoff, H.: Kinetics, SOA yields, and chemical composition of secondary organic aerosol from β-caryophyllene ozonolysis with and without nitrogen oxides between 213 and 313 K, Atmos. Chem. Phys., 22, 6001-6020, 10.5194/acp-22-6001-2022, 2022b.

Gao, L., Buchholz, A., Li, Z., Song, J., Vallon, M., Jiang, F., Möhler, O., Leisner, T., and Saathoff, H.: Volatility of Secondary Organic Aerosol from β-Caryophyllene Ozonolysis over a Wide Tropospheric Temperature Range, Environmental Science & Technology, 57, 8965-8974, 10.1021/acs.est.3c01151, 2023.

Huang, W., Saathoff, H., Pajunoja, A., Shen, X., Naumann, K. H., Wagner, R., Virtanen, A., Leisner, T., and Mohr, C.: α-Pinene secondary organic aerosol at low temperature: chemical composition and implications for particle viscosity, Atmos. Chem. Phys., 18, 2883-2898, 10.5194/acp-18-2883-2018, 2018.

Lane, T. E., Donahue, N. M., and Pandis, S. N.: Simulating secondary organic aerosol formation using the volatility basis-set approach in a chemical transport model, Atmospheric Environment, 42, 7439-7451, https://doi.org/10.1016/j.atmosenv.2008.06.026, 2008.

Lee, B. H., Lopez-Hilfiker, F. D., Mohr, C., Kurtén, T., Worsnop, D. R., and Thornton, J. A.: An Iodide-Adduct High-Resolution Time-of-Flight Chemical-Ionization Mass Spectrometer: Application to Atmospheric Inorganic and Organic Compounds, Environmental Science & Technology, 48, 6309-6317, 10.1021/es500362a, 2014.

Li, Y., Pöschl, U., and Shiraiwa, M.: Molecular corridors and parameterizations of volatility in the chemical evolution of organic aerosols, Atmos. Chem. Phys., 16, 3327-3344, 10.5194/acp-16-3327-2016, 2016.

Lopez-Hilfiker, F. D., Iyer, S., Mohr, C., Lee, B. H., D'Ambro, E. L., Kurtén, T., and Thornton, J. A.: Constraining the sensitivity of iodide adduct chemical ionization mass spectrometry to multifunctional organic molecules using the collision limit and thermodynamic stability of iodide ion adducts, Atmos. Meas. Tech., 9, 1505-1512, 10.5194/amt-9-1505-2016, 2016a.

Lopez-Hilfiker, F. D., Mohr, C., Ehn, M., Rubach, F., Kleist, E., Wildt, J., Mentel, T. F., Lutz, A., Hallquist, M., Worsnop, D., and Thornton, J. A.: A novel method for online analysis of gas and particle composition: description and evaluation of a Filter Inlet for Gases and AEROsols (FIGAERO), Atmos. Meas. Tech., 7, 983-1001, 10.5194/amt-7-983-2014, 2014.

Lopez-Hilfiker, F. D., Mohr, C., D'Ambro, E. L., Lutz, A., Riedel, T. P., Gaston, C. J., Iyer, S., Zhang, Z., Gold, A., Surratt, J. D., Lee, B. H., Kurten, T., Hu, W. W., Jimenez, J., Hallquist, M., and Thornton, J. A.: Molecular Composition and Volatility of Organic Aerosol in the Southeastern U.S.: Implications for IEPOX Derived SOA, Environmental Science & Technology, 50, 2200-2209, 10.1021/acs.est.5b04769, 2016b.

Murphy, B. N. and Pandis, S. N.: Simulating the Formation of Semivolatile Primary and Secondary Organic Aerosol in a Regional Chemical Transport Model, Environmental Science & Technology, 43, 4722-4728, 10.1021/es803168a, 2009.
Ng, N. L., Kroll, J. H., Keywood, M. D., Bahreini, R., Varutbangkul, V., Flagan, R. C., Seinfeld, J. H., Lee, A., and Goldstein, A. H.: Contribution of First- versus Second-Generation Products to Secondary Organic Aerosols Formed in the Oxidation of Biogenic Hydrocarbons, Environmental Science & Technology, 40, 2283-2297, 10.1021/es052269u, 2006.
Riva, M., Rantala, P., Krechmer, J. E., Peräkylä, O., Zhang, Y., Heikkinen, L., Garmash, O., Yan, C., Kulmala, M., Worsnop, D., and Ehn, M.: Evaluating the performance of five different chemical ionization techniques for detecting gaseous oxygenated organic species, Atmos. Meas. Tech., 12, 2403-2421, 10.5194/amt-12-2403-2019, 2019.
Stark, H., Yatavelli, R. L. N., Thompson, S. L., Kang, H., Krechmer, J. E., Kimmel, J. R., Palm, B. B., Hu, W., Hayes, P. L., Day, D. A., Campuzano-Jost, P., Canagaratna, M. R., Jayne, J. T., Worsnop, D. R., and Jimenez, J. L.: Impact of Thermal Decomposition on Thermal Desorption Instruments: Advantage of Thermogram Analysis for Quantifying Volatility Distributions of Organic Species, Environmental Science & Technology, 51, 8491-8500, 10.1021/acs.est.7b00160, 2017.
Thornton, J. A., Mohr, C., Schobesberger, S., D'Ambro, E. L., Lee, B. H., and Lopez-Hilfiker, F. D.: Evaluating Organic Aerosol Sources and Evolution with a Combined Molecular Composition and Volatility Framework Using the Filter Inlet for Gases and Aerosols (FIGAERO), Accounts of Chemical Research, 53, 1415-1426, 10.1021/acs.accounts.0c00259, 2020.
Tsimpidi, A. P., Karydis, V. A., Zavala, M., Lei, W., Molina, L., Ulbrich, I. M., Jimenez, J. L., and Pandis, S. N.: Evaluation of the volatility basis-set approach for the simulation of organic aerosol formation in the Mexico City metropolitan area, Atmos. Chem. Phys., 10, 525-546, 10.5194/acp-10-525-2010, 2010.
Yang, X., Ren, S., Wang, Y., Yang, G., Li, Y., Li, C., Wang, L., Yao, L., and Wang, L.: Volatility Parametrization of Low-Volatile Components of Ambient Organic Aerosols Based on Molecular Formulas, Environmental Science & Technology, 57, 11595-11604, 10.1021/acs.est.3c02073, 2023.
Ye, Q., Wang, M., Hofbauer, V., Stolzenburg, D., Chen, D., Schervish, M., Vogel, A., Mauldin, R. L., Baalbaki, R., Brilke, S., Dada, L., Dias, A., Duplissy, J., El Haddad, I., Finkenzeller, H., Fischer, L., He, X., Kim, C., Kürten, A., Lamkaddam, H., Lee, C. P., Lehtipalo, K., Leiminger, M., Manninen, H. E., Marten, R., Mentler, B., Partoll, E., Petäjä, T., Rissanen, M., Schobesberger, S., Schuchmann, S., Simon, M., Tham, Y. J., Vazquez-Pufleau, M., Wagner, A. C., Wang, Y., Wu, Y., Xiao, M., Baltensperger, U., Curtius, J., Flagan, R., Kirkby, J., Kulmala, M., Volkamer, R., Winkler, P. M., Worsnop, D., and Donahue, N. M.: Molecular Composition and Volatility of Nucleated Particles from α-Pinene Oxidation between −50 °C and +25 °C, Environmental Science & Technology, 53, 12357-12365, 10.1021/acs.est.9b03265, 2019.